Journal of Inorganic and Organometallic Polymers and Materials (2018) 28:2196–2205
https://doi.org/10.1007/s10904-018-0914-8

Embedded of Nanogel into Multi-responsive Hydrogel Nanocomposite for Anticancer Drug Delivery

Ghasem Rezanejade Bardajee[1] · Samaneh Sadat Hosseini[1] · Somayeh Ghavami[1]

Received: 23 February 2018 / Accepted: 9 July 2018 / Published online: 28 July 2018

Abstract
Hydrogels, nanogels, and nanocomposites show increasing potential for application in drug delivery systems due to their good chemical and physical properties. Therefore, we were encouraged to combine them to produce a new compound with unique properties for drug release systems. To this aim, we first prepared poly [(*N*-isopropylacrylamide)-co-(2-dimethylamino ethyl methacrylate) nanogel by copolymerization processes and then added it into the solution of poly (2-dimethylamino ethyl methacrylate)] grafted onto salep. Through dropwise addition of mixed aqueous solution of iron salts into the prepared polymeric solution, a novel hydrogel nanocomposite with excellent pH, thermo, and magnetic responsive was fabricated. The obtained hydrogel nanocomposite were characterized by Fourier transform infrared spectroscopy, thermo gravimetric analysis, X-ray diffraction, scanning electron microscopy, vibrating sample magnetometer, and atomic force micrographs. The dependence of swelling properties of hydrogel nanocomposite on the temperature, pH, and magnetic field were investigated. The release behavior of doxorubicin hydrochloride (DOX) drug from DOX loaded into synthesized hydrogel nanocomposite was investigated at different pHs, temperatures, and magnetic field. In addition, the drug release behavior from obtained hydrogel nanocomposite was monitored via different kinetic models. Lastly, the toxicity of the DOX and DOX-loaded hydrogel nanocomposite were studied on MCF-7 cells at different times. These results suggested that the obtained hydrogel nanocomposite might have high potential applications in drug delivery systems.

Keywords Swelling · Hydrogel · Nanogel · Nanocomposite · Drug release

1 Introduction

Cancer is a major life-treating disease due to its high incidence rate and mortality rate [1–3]. Over the last years, the use of anticancer drugs (also called cytostatic or anti-neoplastic drugs) such as doxorubicin hydrochloride (DOX), to treat human cancers has remarkably increased [4, 5]. These compounds affect on both tumor cells and normal growing cells during the chemotherapy and cause adverse side effects like hair loss, anemia, nausea and vomiting etc. [3–5]. Therefore, their clinical applications have been limited [4]. To increase the effectiveness of anticancer drugs with little or no effect on normal cells, many biocompatible and biodegradable controlled drug delivery systems were developed [6, 7]. In these systems, the loaded drug was released in the cancer site without leaking into other sites [8–10]. One of the most important and interesting drug delivery systems is multi-responsive hydrogels. They have different groups into their three dimensional polymeric networks and could respond to specific varieties in the external environment, including temperature, pH, pressure, electric field, magnetic field, and light [9–11]. More recently, multi-responsive hydrogels based polysaccharides (e.g. starch, salep, alginate, carrageenan) have attracted much attention due to their high water swelling, biocompatibility, biodegradability, eco-friendliness, low cost, and biological functions [12, 13]. However, a general problem with these hydrogels is their rapid release of encapsulated drugs and low mechanical property.

A remedy proposed to address first issue is the incorporation of micro or nanogels containing anticancer drug into multi-responsive hydrogels. For example, Gil et al. reported the ability of pH- and temperature-responsive bioresorbable poly(ethylene glycol)–poly(b-aminoester urethane) hydrogels containing cisplatin-bearing chondroitin sulfate

✉ Ghasem Rezanejade Bardajee
rezanejad@pnu.ac.ir

[1] Department of Chemistry, Payame Noor University, PO BOX 19395-3697, Tehran, Iran

nanogels (CS-nanogels) to slowly release of cancer cell-specific delivery of cisplatin (CDDP) at pH 7.4 and trigger release of CDDP at pH 5 [14]. In the other work, Molinos et al. showed that the hybrid dextrin hydrogel encapsulating dextrin nanogel could release of the dextrin nanogel over an extended period, paralleling the mass loss curve due to the degradation of the material [15]. Lehmann et al. description the mobility of nanoscopic dextran tracers within the poly(acrylamide) hydrogel matrix including micrometer-sized poly(*N*-isopropylacrylamide) microgel [16]. They found that the microgel beads could hinder the mobility of dextran tracers comparing to those in free beads and in the surrounding gel matrix.

Many efforts have been focused on increasing the mechanical properties of hydrogels using nanoparticle (NPs) as a highly multifunctional crosslinking agent [17, 18]. Among various types of NPs that can be used for crosslinking of hydrogel, Fe_3O_4 NPs have potential applications due to their accessibility and stability of the +2 and +3 oxidation states [19, 20]. The utmost advantage of using Fe_3O_4 NPs is their strong magnetic properties and low toxicity [21]. Zhou et al. reported an efficient and simple approach to form poly (vinyl alcohol) (PVA) gel using Fe_3O_4 NPs as a crosslinking agent [22]. In this approach, the Fe_3O_4 NPs and cross-link of PVA chains was prepared by mixing aqueous solution of iron salts and PVA solution and then dropwise addition of it into alkaline solution. In this process, Fe_3O_4 NPs created physical crosslinking with polymer chains during hydrogen bond, ionic bond or coordination bond. Recently, we used the same approach to synthesize different biocompatible hydrogel nanocomposites based on salep, Kappa carrageenan, and starch [23–25]. These hydrogel nanocomposites demonstrated exceptional characteristics comparing to free hydrogel and Fe_3O_4 NPs. By taking these advantages, it is necessary to enhance drug release behaviors of hydrogel nanocomposites.

The above reported results encouraged us to embedding nanogel into multi responsive hydrogel nanocomposite for creating a novel drug delivery system. To the best of our knowledge, there is no reported about this in the literatures. In this study, nanogel was fabricated through copolymerization of *N*-isopropylacrylamide (NIPAM) and acrylic acid (AA). This newly formed nanogel added into the solution of graft copolymerization of PAA onto salep and Fe ions. In order to form simultaneously crosslinking polymeric network and Fe_3O_4 NPs, the ammoniac solution was added into the mixture. The properties of the samples were analyzed and characterized using Fourier transform infrared spectroscopy (FT-IR), thermo gravimetric analysis (TGA), X-ray diffraction (XRD), scanning electron microscopy (SEM), vibrating sample magnetometer (VSM), and atomic force micrographs (AFM). The multi-responsive swelling behavior of sample was investigated at different times, temperatures, and pHs. More importantly, DOX drug was also studied to appreciate potential of the obtained hydrogel nanocomposite for use as controlled release drug systems.

2 Experimental

2.1 Materials

Salep was purchased from a supplier in Kordestan, Iran ($M_n = 1.17 \times 10^6$ g/mol, $M_w = 1.64 \times 10^6$ g/mol (high M_w), PDI = 1.39, eluent = water, flow rate = 1 mL/min, acquisition interval = 0.43 s from GPC results). Reagents including sodium dodecyl sulfate (SDS), *N,N*-methylenebisacrylamide (MBA), *N*-isopropylacrylamide (NIPAM), AA, ferric chloride hexahydrate ($FeCl_3{\cdot}6H_2O$), ferrous chloride tetrahydrate ($FeCl_2{\cdot}4H_2O$), and DOX were purchased from Sigma-Aldrich, Germany. Ammonium persulfate (APS) was obtained from Fluka, USA. All chemicals were at least of analytical reagent grade and used as received. Double distilled water was used in all the processes of aqueous solution preparations and washings.

2.2 Characterization

FT-IR spectra were achieved in the wave number ranging from 400 to 4000 cm^{-1} using a Jasco 4200 FT-IR spectrophotometer. TGA was measured for powder samples (about 10 mg) using a TA instrument 2050 thermo-gravimetric (TG) analyzer at a heating rate 20 °C/min, nitrogen flux. SEM examinations were obtained by a Hitachi S-5200 SEM at an acceleration voltage of 10 kV. AFM were collected using an AFM; SPI3800, Seiko Instruments, Japan. XRD was performed using a D/Max-IIIA XRD analyzer equipped with a Cu Kα monochromatic radiation source. Vibrating sample magnetometer (VSM) was performed using the Model 880 from ADE technologies, USA. The UV–Vis absorption spectra of the samples were recorded on a Shimadzu UV–Visible 1650 PC spectrophotometer.

2.3 Preparation of PAN-Nanogel and DOX/PAN-Nanogel

For the synthesis of PAN-nanogel, MBA (0.1 g), SDS (0.05 g), AA (4 mL), and NIPAM (0.5 g) were added into the beaker containing 45 mL double distilled water. The formation mixture was stirred for 30 min under Ar purge at 80 °C. Then, APS (0.03 g in 2 mL water) was added and the reaction was allowed to proceed for 4 h. At last, the product was centrifuged, was washed with water, and was dried at 40 °C.

DOX/PAN-nanogel was prepared in a similar fashion with 1 mL DOX solution before addition of APS. The final product was analyzed using an UV–Vis spectrometer to

detect the absorption of the media for indirect determination of the DOX encapsulation efficiency.

2.4 Preparation of PAN-Nanogel-PAS-Fe_3O_4 NPs Hydrogel Nanocomposite and DOX/PAN-Nanogel-PAS-Fe_3O_4 NPs Hydrogel Nanocomposite

0.2 g of salep was dispersed under stirring in 25 mL of double distilled water at 80 °C. 4 mL of AA solution and 5 mL of APS (0.2 g in 5 mL water) were added into homogeneous viscous of salep and the reaction was continued for 30 min at 80 °C. Then, the reaction mixture was cooled and was poured into 100 mL of ethanol, was dried under vacuum at 40 °C, and was subjected to the extraction with the double distilled water to remove uncrosslinked polymer and/or residual monomer. Then, 15 mL of PAN-nanogel was added to the reaction and was stirred for 45 min at 80 °C. The solution was cooled at room temperature. A solution of $FeCl_3/FeCl_2$ (0.48/0.16 in 20 mL water) was added into prepped mixture by dropping funnel simultaneously under constant stirring. The addition was continued for a periods while the temperature was maintained at room temperature. After complete addition of $FeCl_3/FeCl_2$ solutions, the admixture was stirred at room temperature for additional 30 min. After that, 20 mL of NH_4OH was added to the solution. The solid phase was extracted, was dried, and was stored in the absence of moisture, heat, and light to further characterization.

The DOX/PAN-nanogel-PAS-Fe_3O_4 NPs hydrogel nanocomposite was synthesized by the above mentioned method and using DOX/PAN-nanogel instead of PAN-nanogel.

2.5 Swelling Study

For the swelling experiments, a tea bag (i.e., a 100.00-mesh nylon screen) containing 0.5 g of sample was immersed in 50 mL solution. After a pre determined interval, the swollen tea bag was separated and was hanged until the last drop of double distilled water was fallen down. The swelling degree (g/g) was calculated based on the following equation [12]:

$$\text{Swelling degree (g/g)} = (\text{Weight of swollen gel}/\text{Weight of dried gel}) - 1$$

The swelling behavior of sample under load was measured by potting a cylindrical solid weight (Teflon, d = 60 mm of variable height) with desired load (applied pressure 0.3 and 0.9 psi) onto 0.5 g sample. This sample was uniformly placed on the surface of a polyester gauze which was pot in a Petri dish ($d = 118$ mm and $h = 12$ mm) containing double distilled water. The mass of swollen sample was weighted and the swelling degree was calculated by above equation.

2.6 Drug Release Studies

DOX was used as a model drug to investigate the controlled release of the PAN-nanogel-PAS-Fe_3O_4 NPs hydrogel nanocomposite. 1 mL of the as-prepared DOX/PAN-nanogel-PAS-Fe_3O_4 NPs hydrogel nanocomposite was taken into a dialysis bag and immersed in 80 mL of buffer (pH 5.3 and 7.4) with different temperatures (37 and 42 °C). At regular time-points, 2 mL of solution was collected and refreshed with 2 mL of fresh buffer. The concentration of DOX was monitored by the UV–Vis spectrophotometer and calculated from the standard curve of DOX.

2.7 In Vitro Cytotoxicity

The cell toxicity of the synthesized hydrogel nanocomposite was investigated onto Michigan Cancer Foundation-7 (MCF-7) by 3-(4, 5-dimethyl-thiazole-2-yl)-2, 5-diphenyl tetrazolium (MTT) assay. The 96 well plates with a density of 1×10^4 cells/cm^2 were seeded up to reach 90% confluency. Then the cells were washed with PBS buffer after and then the hydrogel nanocomposite (0.01 mg/mL) was added into it. These cells were incubated for 24 h and then were treated with PBS. After that, they were incubated with 100 µL supplemented DMEM and 20 µL of 5 mg/mL MTT. Finally, a microplate reader was used to measure the absorbance of media at a wavelength of 570 nm. To more investigations, the cell toxicity of DOX/PAN-nanogel-PAS-Fe_3O_4 NPs hydrogel nanocomposite and free DOX were tested with the same way. As a control, the cells without treatment were used. Cell viability percentage was calculated with below equation:

$$\text{Cell viability \%} = (\text{Sample absorbance}/\text{Control absorbance}) \times 100$$

3 Results and Discussions

3.1 Synthesis Mechanism

The schematic synthetic route of PAN-nanogel-PAS-Fe_3O_4 NPs hydrogel nanocomposite is illustrated in Scheme 1. In the first step, PAN-nanogel was obtained by the copolymerization process between NIPAM and AA monomers in the presence of APS at 80 °C. Three dimensional polymeric network structures were shaped after addition of MBA to this solution. In order to separate polymeric network and formation of nanogel, SDS was added. In this step, the appearing of turbidity in the solution confirmed the formation of nanogel. In another reaction container, AA as a monomer

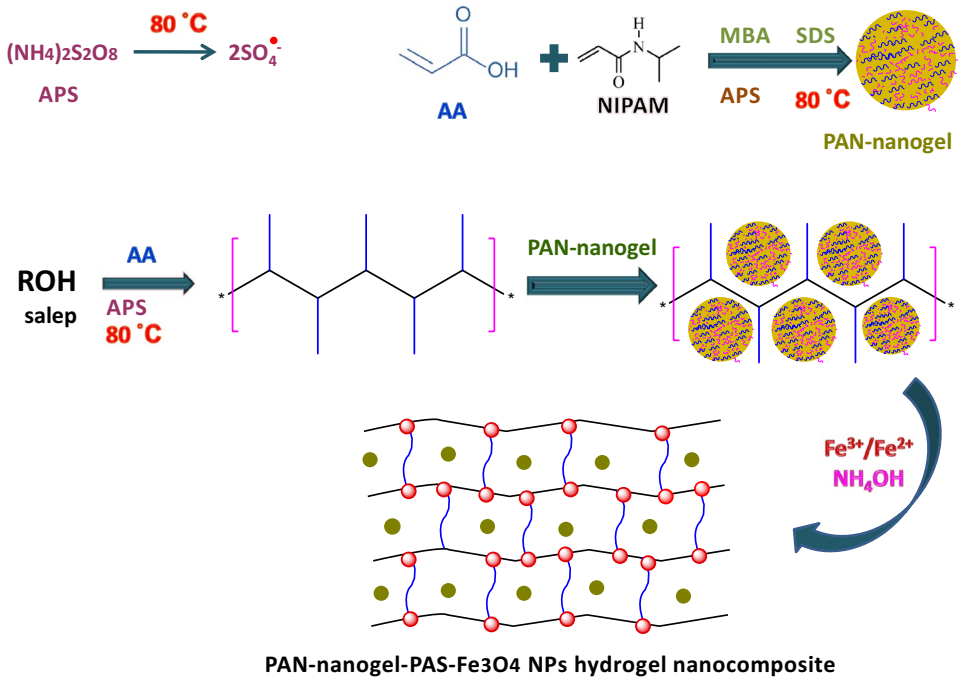

Scheme 1 Proposed mechanism for preparation of PAN-nanogel-PAS-Fe_3O_4 NPs hydrogel nanocomposite

was mixed with salep as a backbone and graft copolymerization process of AA onto salep was happen. Afterward, PAN-nanogel was added to the graft copolymerization solution. In order to form hydrogel nanocomposite, iron sources were used due to ability of Fe ions to chelate with nitrogen and oxygen atoms [23, 24]. Therefore, the prepared Fe_3O_4 NPs act as crosslinking agents in three-dimensional polymeric network of PAN-nanogel-PAS-Fe_3O_4 NPs hydrogel nanocomposite [25].

3.2 Characterization

The related FT-IR spectra of the salep, PAA, PNIPAM, PAN-nanogel, and PAN-nanogel-PAS-Fe_3O_4 NPs hydrogel nanocomposite are given in Fig. 1a. In the spectrum of salep, the bands at 3265 and 1690 cm^{-1} could be attributed to hydroxyl functional groups and stretching modes of the carboxyl groups, respectively. The FT-IR spectrum of PAA showed the carbonyl vibrations in the ester functional groups at 1720 cm^{-1}. The FT-IR spectrum of the PNIPAM revealed the typical characteristic bands of the N–H and C=O stretching of the amide groups at 3500 and 1635 cm^{-1}. The FT-IR spectrum of PAN-nanogel indicate that the characterization vibrations of both PAA and PNIPAM at 3500, 1720, and 1635 cm^{-1} without any significantly changed after the copolymerization processes. Differences were detected on the intensity of all aforementioned bands, which decreased after the copolymerization processes because of the significant decrease in their amount. All the characterization vibrations of salep, PAA, and PAN-nanogel were observed in the FT-IR spectrum of PAN-nanogel-PAS-Fe_3O_4 NPs hydrogel nanocomposite. These data, in sum, confirmed the formation of the PAN-nanogel-PAS-Fe_3O_4 NPs hydrogel nanocomposite.

The TGA profiles of salep, PAA, PNIPAM, PAN-nanogel, and PAN-nanogel-PAS-Fe_3O_4 NPs hydrogel nanocomposite are shown in Fig. 1b for the entire temperature range. The initial stage weight loss for all samples in the range of 35–100 °C is attributed to removal of residual moisture in samples. The weight loss of salep between 260 and 650 °C corresponds to the dehydration of saccharide rings and breaking of C–O–C bonds in the polymeric chains. Degradation of PAA and PNIPAM at 200–500 and 200–620 °C, respectively, are attributed to decomposition of carboxyl and amide side groups of the polymers, resulting to emission of ammonia, carbon monoxide and carbon dioxide. Degradation of PAN-nanogel between 180 and 410 °C is essentially assigned to random scission of copolymer chains. Decomposition of PAN-nanogel-PAS-Fe_3O_4 NPs hydrogel nanocomposite is happen in the range of 180–610 °C. The rise in thermal stability of PAN-nanogel-PAS-Fe_3O_4 NPs hydrogel nanocomposite comparing to PAN-nanogel is proportional to concentration of Fe_3O_4 NPs in the hydrogel nanocomposite matrix. Therefore, Fe_3O_4 NPs increase thermal stability of the polymeric matrix in the hydrogel nanocomposite structure.

SEM micrographs of the synthesized PAN-nanogel-PAS-Fe_3O_4 NPs hydrogel nanocomposite in comparison with the PAN-nanogel are presented in Fig. 2. Similar microstructural features are observable on the fracture surfaces of these samples. However, SEM observations revealed that PAN-nanogel-PAS-Fe_3O_4 NPs hydrogel nanocomposite had more

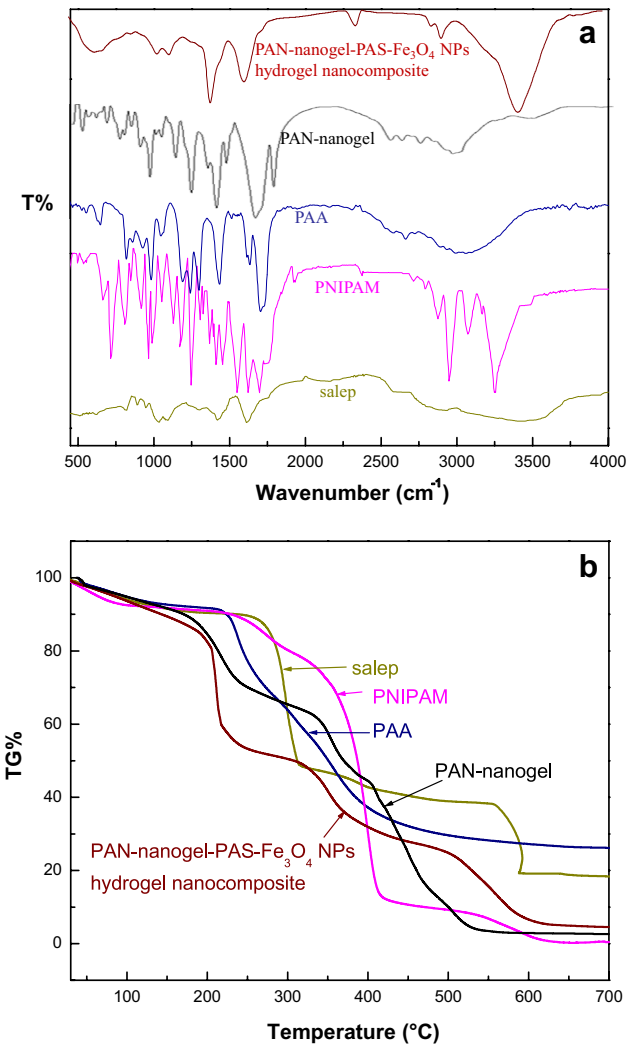

Fig. 1 **a** FT-IR spectra and **b** TGA of salep, PAA, PNIPAM, PAN-nanogel, and PAN-nanogel-PAS-Fe_3O_4 NPs hydrogel nanocomposite

porosity than PAN-nanogel. This might be due to the fact that the Fe_3O_4 NPs can properly act as a crosslinking agent.

Further investigations on about the morphology and size distribution of the PAN-nanogel and PAN-nanogel-PAS-Fe_3O_4 NPs hydrogel nanocomposite were done by AFM (Fig. 2). The results revealed the spherical morphology with a smooth surface and diameter of about 8.13 nm for PAN-nanogel and 21.47 nm for PAN-nanogel-PAS-Fe_3O_4 NPs hydrogel nanocomposite.

In order to confirm the presence of Fe_3O_4 NPs in the PAN-nanogel-PAS-Fe_3O_4 NPs hydrogel nanocomposite sample, XRD of PAN-nanogel-PAS-Fe_3O_4 NPs hydrogel nanocomposite was taken out and then it was compared with the XRD of PAN-nanogel (Fig. 3). The XRD pattern of PAN-nanogel-PAS-Fe_3O_4 NPs hydrogel nanocomposite exhibited the characteristic reflections of Fe_3O_4 NPs at $2\theta = 30.1$, 35.4, 43.0, 53.5, 57.0 and 62.5 °C, while the XRD pattern of PAN-nanogel didn't show any characteristic peaks of Fe_3O_4 NPs. The above observations show that the Fe_3O_4 NPs were successfully fabricated into the hydrogel nanocomposite network [26]. The average size of Fe_3O_4 NPs determined by XRD (Scherrer's formula) was found to be 16.2 nm.

The magnetic properties of PAN-nanogel-PAS-Fe_3O_4 NPs hydrogel nanocomposite was investigated using VSM analysis at room temperature, as shown in Fig. 3. The magnetization curve show small ferromagnetic properties over the applied magnetic field owing to the narrow hysteresis ring. The values of magnetization saturation (M_s), field reversals (H_c), and residual magnetization (M_r) were calculated about 0.06 emu/g, −150 to 150 Oe, and −45 to 45 emu/g, respectively. This magnetic property is proper for hydrogel nanocomposite in biomedical applications.

3.3 Swelling Study

For the practical application, the swelling behavior of the prepared hydrogel nanocomposite needs to be evaluated. The swelling behavior of the PAN-nanogel-PAS-Fe_3O_4 NPs hydrogel nanocomposite as a function of time in double distilled water at 25 °C is shown in Fig. 4. It is observed that there is a rapid swelling in the initial 75 min, owing to the diffusion of water molecules into it [23]. However, after 75 min no significant swelling was observed in the hydrogel nanocomposite revealing the attainment of equilibrium over a period of 75 min. Therefore, the PAN-nanogel-PAS-Fe_3O_4 NPs hydrogel nanocomposite shows ideal swelling behavior favoring the usage of it for drug delivery application.

We also examined the effect of AUL on the swelling degree of PAN-nanogel-PAS-Fe_3O_4 NPs hydrogel nanocomposite in double distilled water via two different pressures (0.3 and 0.9 psi) (Fig. 4). It was observed that the swelling degree of PAN-nanogel-PAS-Fe_3O_4 NPs hydrogel nanocomposite decreased when the amount of apply pressure increased. It can be attributed to the decrease in pores dimensions and pores deformation. Nevertheless, the swelling property of PAN-nanogel-PAS-Fe_3O_4 NPs hydrogel nanocomposite was maintained even at high pressures, which is excellent property in the producing of absorbents such as pad and diapers [23–25].

To investigate the influence of medium temperature on the swelling degree of PAN-nanogel-PAS-Fe_3O_4 NPs hydrogel nanocomposite, 0.5 g of this sample was placed in double distilled water with different temperatures for 75 min. As shown in Fig. 5a, the swelling degree of PAN-nanogel-PAS-Fe_3O_4 NPs hydrogel nanocomposite at higher temperatures are lower than those of lower temperatures. It is due to the collapse of polymeric network at higher temperatures [23]. This confirms in this case that the temperature of medium

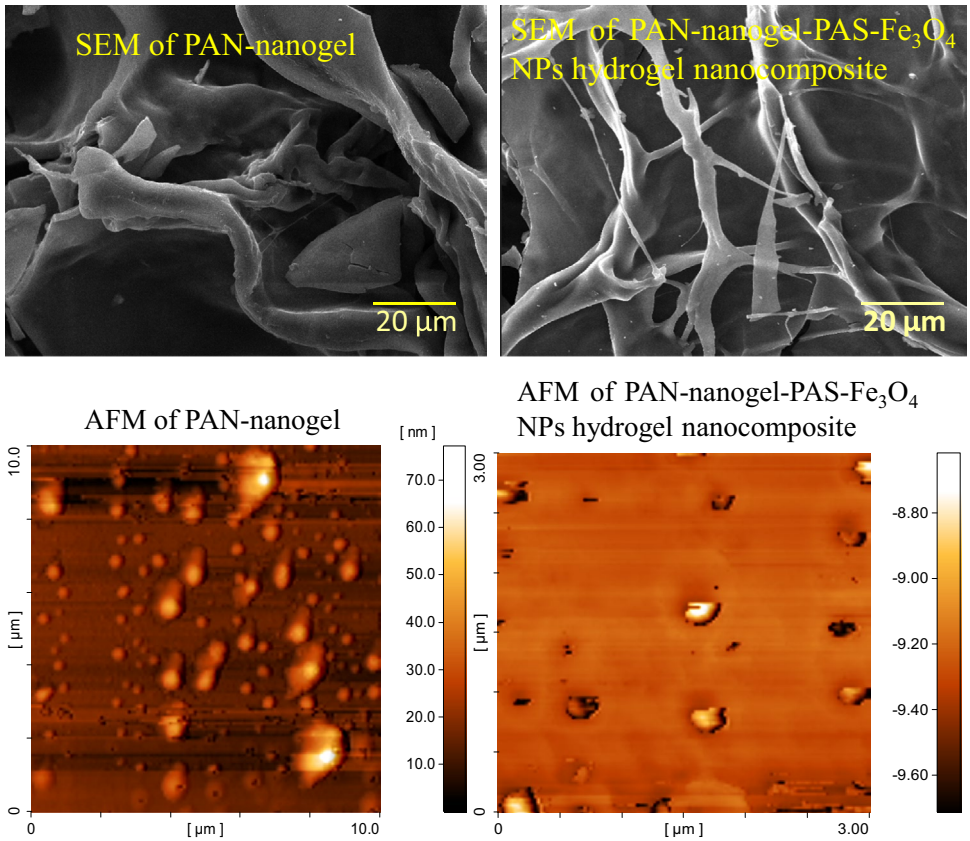

Fig. 2 SEM and AFM of PAN-nanogel and PAN-nanogel-PAS-Fe_3O_4 NPs hydrogel nanocomposite

does severely affect on the swelling degree of the hydrogel nanocomposite.

The influence of various pHs on the swelling behavior of PAN-nanogel-PAS-Fe_3O_4 NPs hydrogel nanocomposite was investigated to reveal its pH sensitivity. To this aim, the swelling degree of PAN-nanogel-PAS-Fe_3O_4 NPs hydrogel nanocomposite was measured by placing 0.5 g of it in different pHs at 25 °C for 75 min. As exhibited in Fig. 5b, the swelling degree of PAN-nanogel-PAS-Fe_3O_4 NPs hydrogel nanocomposite is less at pH 2, increases sharply from pH 2 to 6, but again decreases sharply at pH > 6. By increasing pH from 2 to 6, the electrostatic repulsion force between ionization groups leading to increase swelling degree. However, for pH > 6, high concentration of OH in solution cause to reduce the osmotic pressure and result to decrease swelling ratios [27, 28].

The sensitivity of the prepared hydrogel nanocomposite to the magnetic field was also determined, as shown in Fig. 5c. The swelling degree of PAN-nanogel-PAS-Fe_3O_4 NPs hydrogel nanocomposite decreases in the presence of magnet. In other words, the PAN-nanogel-PAS-Fe_3O_4 NPs hydrogel nanocomposite has a lower swelling degree in the presence of magnet. This decline may be attributed to collecting of the Fe_3O_4 NPs in the neighbors of magnet, which reduce distance between the Fe_3O_4 NPs and produce close-packed shells of Fe_3O_4 NPs. This phenomenon restrains the water diffusion into polymeric network of hydrogel nanocomposite. It indicates that the PAN-nanogel-PAS-Fe_3O_4 NPs hydrogel nanocomposite is essentially magnetic dependent [23–25].

The inserts in Fig. 5a, b, c show swelling reversibility of PAN-nanogel-PAS-Fe_3O_4 NPs hydrogel nanocomposite to the temperature, pH, and magnetic field, respectively. These results indicate a good repeated swelling–deswelling behavior of PAN-nanogel-PAS-Fe_3O_4 NPs hydrogel nanocomposite under oscillatory temperature (25 and 37 °C), pH (2 and 6), and magnetic field (with magnet and without magnet), which is important for design of drug delivery systems.

3.4 Drug Release

The feasibility of the PAN-nanogel-PAS-Fe_3O_4 NPs hydrogel nanocomposite for drug delivery systems was examined by DOX drug as a model. The loading efficiency was calculated about 87.26%, which suggesting high drug loading content.

The in vitro DOX release profile of PAN-nanogel-PAS-Fe_3O_4 NPs hydrogel nanocomposite was studied by release tests at different conditions. Figure 6a exhibited the influence of pH on the drug release profiles of PAN-nanogel-PAS-Fe_3O_4 NPs hydrogel nanocomposite. The drug release rate was faster at pH 5.3 compared with that at pH 7.4. It

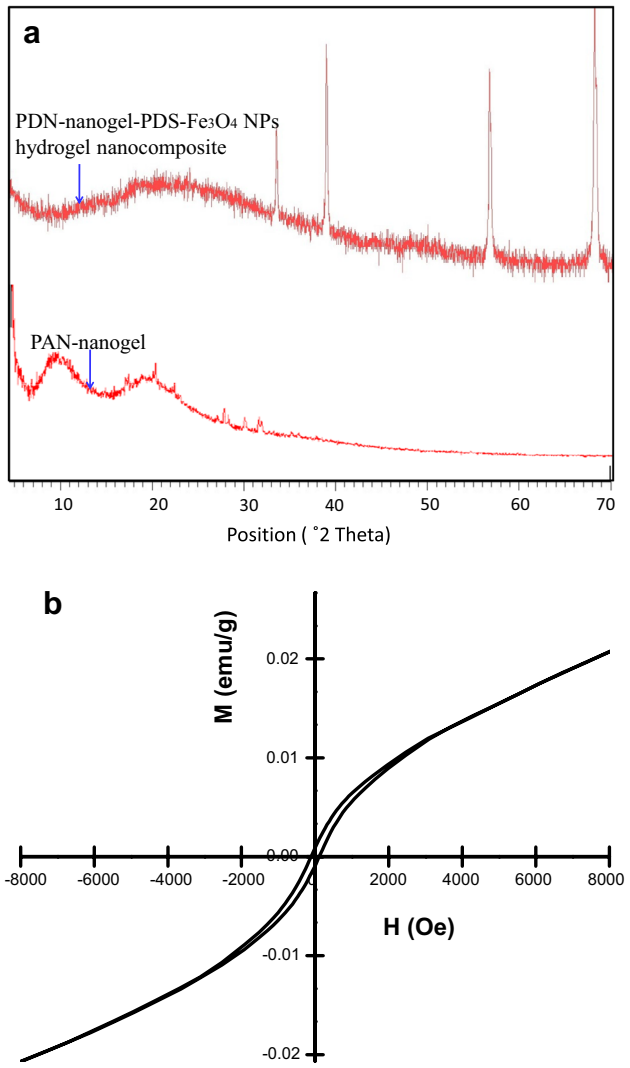

Fig. 3 **a** XRD spectra of PAN-nanogel and PAN-nanogel-PAS-Fe_3O_4 NPs hydrogel nanocomposite and **b** VSM analysis of PAN-nanogel-PAS-Fe_3O_4 NPs hydrogel nanocomposite

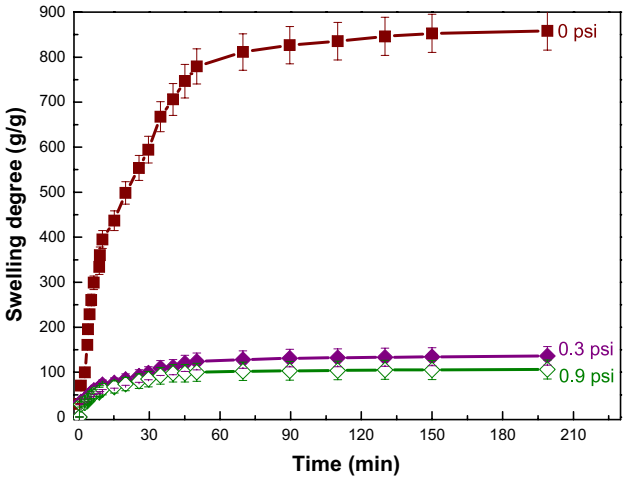

Fig. 4 Time dependence of the swelling degree of PAN-nanogel-PAS-Fe_3O_4 NPs hydrogel nanocomposite at different pressure in double distilled water at 25 °C

can be ascribed to the higher swelling degree of PAN-nanogel-PAS-Fe_3O_4 NPs hydrogel nanocomposite at pH 5.3 and more hydrophilic properties of DOX at a lower pH condition. Since cancer cells have acidic environment, the PAN-nanogel-PAS-Fe_3O_4 NPs hydrogel nanocomposite have a good potential for cancer treatment [29].

Figure 6b shows the release behavior of PAN-nanogel-PAS-Fe_3O_4 NPs hydrogel nanocomposite in pH 5.3 at 37–42 °C. It is clearly seen that the release rate at 42 °C is faster than 37 °C. This phenomenon could be explained by the fact that the PNIPAM shells shrinked at higher temperature [30].

The effect of magnetic field on DOX release from PAN-nanogel-PAS-Fe_3O_4 NPs hydrogel nanocomposite was also evaluated at pH 5.3 and T = 37 °C. PAN-nanogel-PAS-Fe_3O_4 NPs hydrogel nanocomposite showed a magnetic dependence of DOX release as shown in Fig. 6c. In the presence of the magnetic field, the release of DOX from PAN-nanogel-PAS-Fe_3O_4 NPs hydrogel nanocomposite decreased, for example, its release reached up to 62% for 10 days at pH 5.3 and T = 37 °C. The results recommended that the PAN-nanogel-PAS-Fe_3O_4 NPs hydrogel nanocomposite could improve the therapeutic efficacy of DOX drug for tumor cells by sustain drug release in tumor tissue [31].

In order to describe drug release behavior from PAN-nanogel-PAS-Fe_3O_4 NPs hydrogel nanocomposite, the mechanism and kinetics of drug release were investigated by the following equations [32, 33]:

$$\text{Zero - order model}: M_0 - M_t = k_0 t$$

$$\text{First order model}: \ln\left(M_t - M_0\right) = -k_1 t$$

$$\text{Higuchi model}: M_t = k\sqrt{t}$$

$$\text{Hixson–Crowell model}: \left(M_0\right)^{1/3} - \left(M_t\right)^{1/3} = kt$$

$$\text{Korsemeyer–Peppas}: M_t/M_\infty = kt^n$$

where t is the release time; M_t and M_∞ represent the fraction of drug released at time t and infinity, respectively; k is the drug release rate constant, and n display the release mechanism. In the case of cylindrical shape, $n \leq 0.45$ is Fickian release, $0.45 < n < 0.89$ is non-Fickian release; $n \geq 0.85$ is case-II type release. The correlation coefficients (R^2) for all above models are listed in Table 1. Best fit was established by Korsmeyer–Peppas model due to the correlation coefficient closest to 1. The n values were calculated about 1.08 and 0.74 for DOX releases from PAN-nanogel-PAS-Fe_3O_4

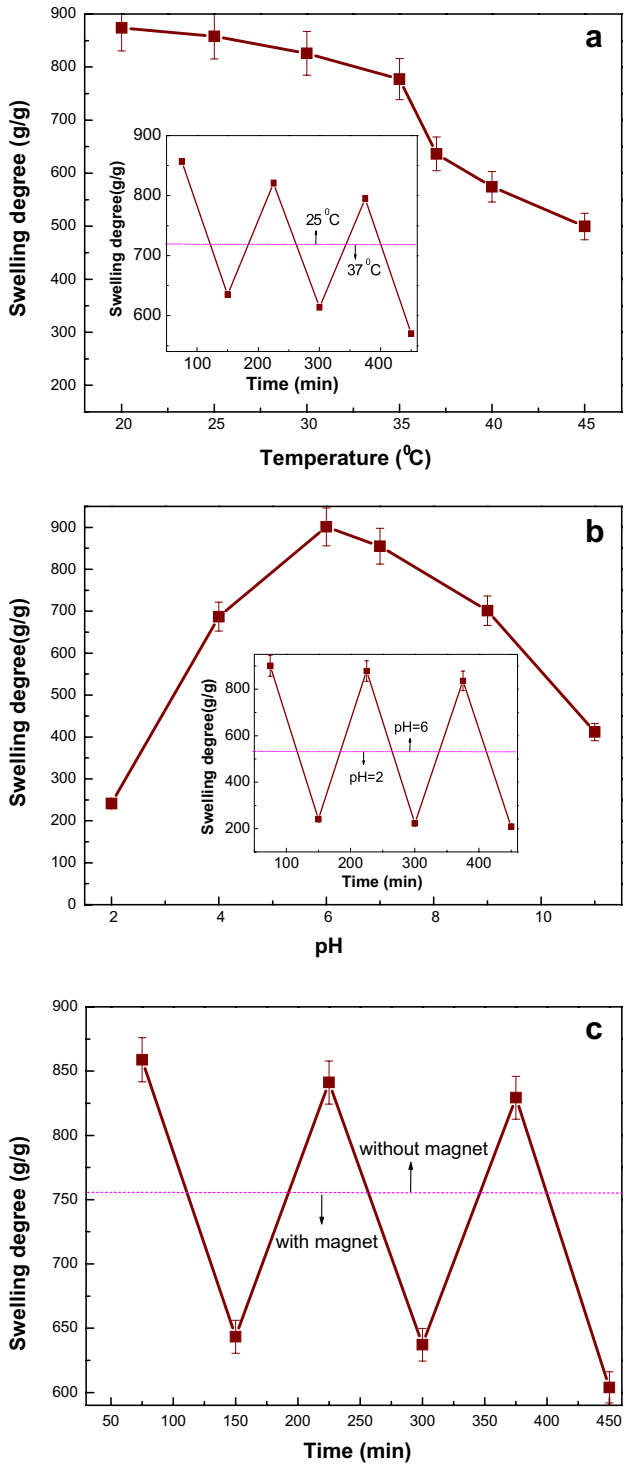

Fig. 5 The effect of **a** temperature, **b** pH, and **c** magnetic-filed on the swelling behavior of PAN-nanogel-PAS-Fe_3O_4 NPs hydrogel nanocomposite

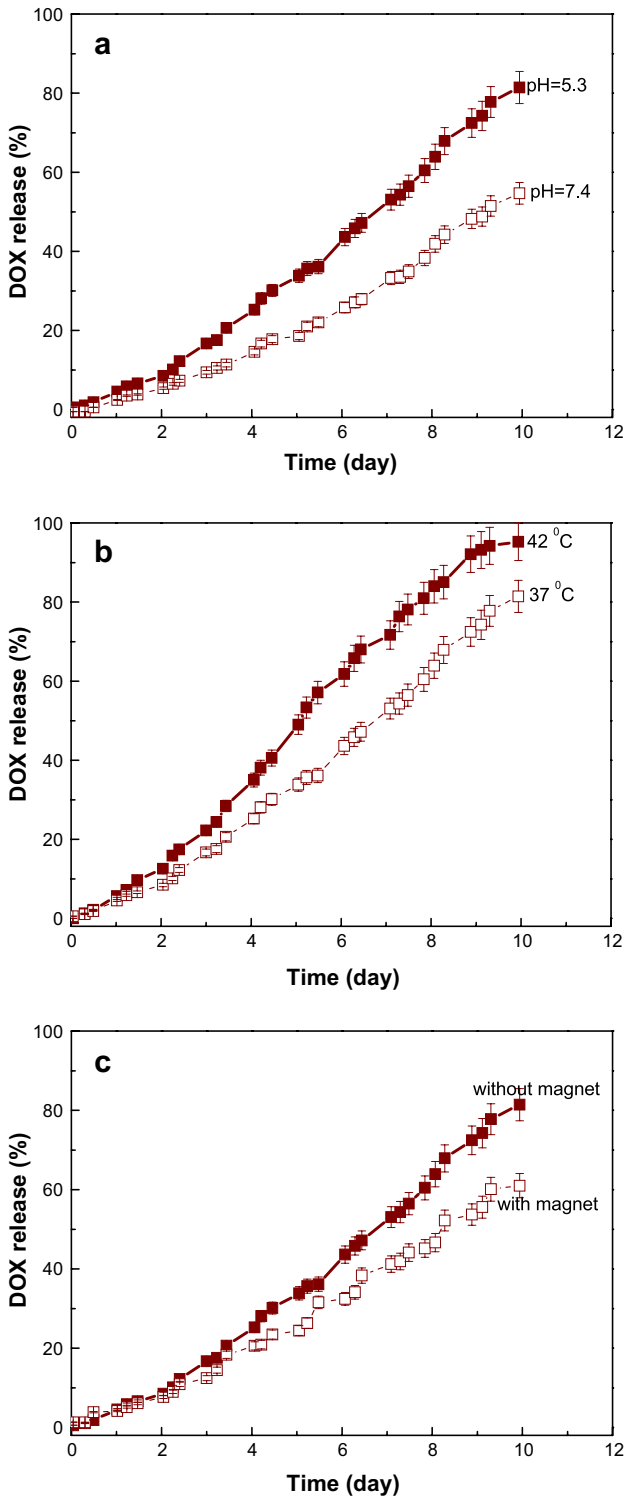

Fig. 6 Effect of **a** pH, **b** temperature, and **c** magnetic field on DOX release from PAN-nanogel-PAS-Fe_3O_4 NPs hydrogel nanocomposite

Table 1 Regression coefficient (R^2) values of different kinetics models for DOX release from DOX/PAN-nanogel-PAS-Fe_3O_4 NPs hydrogel nanocomposite with and without magnetic field

	Without magnetic field	With magnetic field
Zero-order	0.74	0.83
First order	0.85	0.89
Higuchi	0.78	0.76
Hixson–Crowell	0.91	0.89
Korsemeyer–Peppas	0.97	0.98

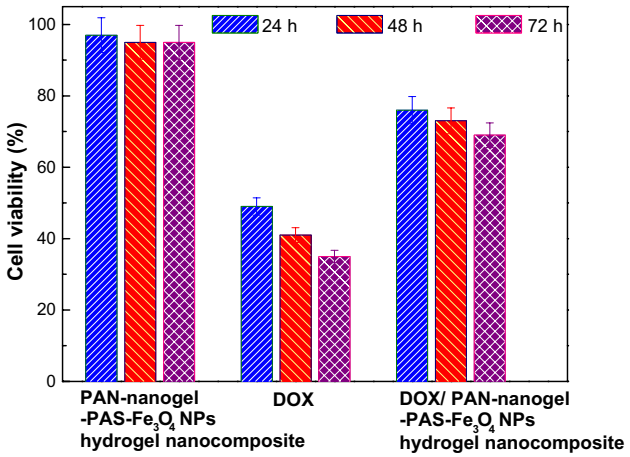

Fig. 7 Cell viability assay of MCF-7 cell exposure to PAN-nanogel-PAS-Fe_3O_4 NPs hydrogel nanocomposite, DOX, and DOX/PAN-nanogel-PAS-Fe_3O_4 NPs hydrogel nanocomposite at different times

NPs hydrogel nanocomposite with magnet and without magnet, respectively. These data revealed that the DOX releases from PAN-nanogel-PAS-Fe_3O_4 NPs hydrogel nanocomposite was non-Fickian with magnet and case-II type release mechanisms without magnet.

3.5 Cytotoxicity Studies

The cell cytotoxicity of PAN-nanogel-PAS-Fe_3O_4 NPs hydrogel nanocomposite, DOX/PAN-nanogel-PAS-Fe_3O_4 NPs hydrogel nanocomposite, and free DOX were studied on MCF-7 cells at different times. The results showed that the PAN-nanogel-PAS-Fe_3O_4 NPs hydrogel nanocomposite had not any cytotoxicity on MCF-7 at various times. In contrast, DOX had a relatively high toxicity on MCF-7 cells. However, the results of the experiments showed that the toxicity of DOX was reduced after its encapsulating in the PAN-nanogel-PAS-Fe_3O_4 NPs hydrogel nanocomposite. This can be due to the slow release of the drug from the hydrogel nanocomposite. These results indicate that synthesized hydrogel nanocomposite can be effectively used as a drug carrier in drug delivery systems (Fig. 7).

4 Conclusion

In this work, PAN-nanogel was successfully embedded in the PAS-Fe_3O_4 NPs hydrogel nanocomposite and introduce as a novel drug delivery system. FT-IR and TGA studies exhibit that the PAN-nanogel-PAS-Fe_3O_4 NPs hydrogel nanocomposite were prepared successfully. SEM images revealed the porous structure of the prepared hydrogel nanocomposite. The VSM results revealed the magnetic properties of the obtained hydrogel nanocomposite. AFM results demonstrated that the PAN-nanogel-PAS-Fe_3O_4 NPs hydrogel nanocomposite had a spherical morphology with a smooth surface. The release experiments showed that the release of DOX drug was accelerated at pH 5.3 with temperature environment 42 °C. In addition, the results of the cytotoxicity test indicate that the toxicity of DOX after its embedding into the hydrogel nanocomposite significantly decreased. The property of prepared hydrogel nanocomposite will be very beneficial for future applications in design drug delivery systems.

Acknowledgements The authors wish to thank Payame Noor University and Iran Nanotechnology Initiative Council for their financial support of this study.

References

1. W. Song, S.N. Musetti, L. Huang, Biomaterials **148**, 16 (2017)
2. J.M. Hotaling, N. Laufer, Z. Rosenwaks, Fertil. Steril. **109**, 4 (2018)
3. C. Rianna, P. Kumar, M. Radmacher, Semin. Cell. Dev. Biol. **73**, 107 (2018)
4. P. Hojman, J. Gehl, J.F. Christensen, B.K. Pedersen, Cell Metab. **27**, 10 (2018)
5. X. Dong, Z. Sun, X. Wang, X. Leng, Nanomedicine **13**, 2271 (2017)
6. W. Zhu, Y. Li, L. Liu, Y. Chen, F. Xi, Int. J. Pharm. **437**, 11 (2012)
7. M. Rasoulzadeh, H. Namazi, Carbohydr. Polym. **168**, 320 (2017)
8. J. Qu, X. Zhao, P.X. Ma, B. Guo, Acta Biomater. **58**, 168 (2017)
9. L. Wei, J. Chen, S. Zhao, J. Ding, X. Chen, Acta Biomater. **58**, 44 (2017)
10. M. Sepantafar, R. Maheronnaghsh, H. Mohammadi, F. Radmanesh, H. Baharvand, Trends Biotechnol. **35**, 1074 (2017)
11. M. Karbarz, M. Mackiewicz, K. Kaniewska, K. Marcisz, Z. Stojek, Appl. Mater. Today **9**, 516 (2017)
12. G.R. Bardajee, Z. Hooshyar, F. Zehtabi, A. Pourjavadi, Iran. Polym. J. **21**, 829 (2012)
13. A. Shalviri, H.K. Chan, G. Raval, M.J. Abdekhodaie, Q. Liu, H. Heerklotz, X.Y. Wu, Colloids Surf. B Biointerfaces **101**, 405 (2013)

14. M.S. Gil, T. Thambi, V.H.G. Phan, S.H. Kim, D.S. Lee, J. Mater. Chem. B **5**, 7140 (2017)
15. M. Molinos, V. Carvalho, D.M. Silva, F.M. Gama, Biomacromolecules **13**, 517 (2012)
16. S. Lehmann, S. Seiffert, W. Richtering, J. Am. Chem. Soc. **134**(38), 15963 (2012)
17. J. Vega-Chacón, M.I.A. Arbeláez, J.H. Jorge, R.F.C. Marques, M. Jafelicci, Mater. Sci. Eng. C **77**, 366 (2017)
18. H.S. Samanta, S.K. Ray, Carbohydr. Polym. **106**, 109 (2014)
19. R. Barbucci, G. Giani, S. Fedi, S. Bottari, M. Casolaro, Acta Biomater. **8**, 4244 (2012)
20. M. Czaun, L. Hevesi, M. Takafujia, H. Ihara, Chem. Commun. (2008). https://doi.org/10.1039/b717721f
21. N. Movagharnezhad, P.N. Moghadam, Polym. Bull. **74**, 4645 (2017)
22. L. Zhou, B. He, F. Zhang, ACS Appl. Mater. Interfaces **4**, 192 (2012)
23. G.R. Bardajee, Z. Hooshyar, F. Rastgo, Colloid Polym. Sci. **291**, 2791 (2013)
24. G.R. Bardajee, Z. Hooshyar, M.J. Asli, F.E. Shahidi, N. Dianatnejad, Mater. Sci. Eng. C **36**, 277 (2014)
25. G.R. Bardajee, Z. Hooshyar, J. Polym. Res. **20**, 298 (2013)
26. K. Huang, S.H. Ehrman, Langmuir **23**, 1419 (2007)
27. X. Yang, X. Zhang, Y. Ma, Y. Huang, Y. Wang, Y. Chen, J. Mater. Chem. **19**, 2710 (2009)
28. R. Salehi, S. Rasouli, H. Hamishehkar, Int. J. Pharm. **487**, 274 (2015)
29. L. Dong, C. Shi, L. Guo, T. Yang, Y. Sun, X. Cui, Ultrason. Sonochem. **36**, 437 (2015)
30. X. Yang, Y. Wang, X. Huang, Y. Ma, Y. Huang, R. Yang, H. Duan, Y. Chen, J. Mater. Chem. **21**, 3448 (2011)
31. X. Cheng, Y. Jin, R. Qi, W. Fan, H. Li, X. Sun, S. Lai, Polymer **101**, 370 (2016)
32. B. Sung, C. Kim, M. Kim, J. Colloid Interface Sci. **450**, 26 (2015)
33. S. Dhanya, D. Bahadur, G.C. Kundu, R. Srivastava, Eur. Polym. J. **49**, 22 (2013)